

A stabilized mixed space-time Proper Generalized Decomposition for the Navier-Stokes equations

Jeferson Wilian Dossa Fernandes^{a,*}, Rodolfo André Kuche Sanches^a, Andrea Barbarulo^b

^a*University of São Paulo, School of Engineering of São Carlos, Structural Engineering Department, Av. Trabalhador São-carlense, 400, São Carlos, São Paulo, Brazil*

^b*Laboratoire MSSMat, CentraleSupélec/CNRS UMR 8579/ Université Paris Saclay, 91190 Gif-sur-Yvette, France*

Abstract

In this paper, a reduced order model based on the Proper Generalized Decomposition (PGD) is applied to the numerical modeling of the incompressible Navier-Stokes equations. Despite of all the advances achieved in numerical analysis in the last decades, the simulation of large-scale, real-time and parametric problems remain a challenge, especially in the Computational Fluid Dynamics (CFD) context. This can be associated to several aspects such as the solution of large algebraic systems, the governing equations nonlinearities and numerical instabilities, computational limitations, among others. This work focuses on providing low cost solution for incompressible flows with low Reynolds numbers by means of a PGD reduced basis built under a space-time decomposition employing a mixed-stabilized approach for two-dimensional flows. The methodology is evaluated with a set of numerical examples, confirming its robustness and precision, as well as a reduction in the number of linear systems to be solved and the run time compared to the standard stabilized finite element approach.

Keywords: Computational Fluid Dynamics; Proper Generalized Decomposition; Reduced Order Modeling; Mixed Formulation; Stabilized Finite Elements.

1. Introduction

Computational fluid dynamics (CFD) is a wide field of research in engineering. Its application ranges from aeronautics, improving aircraft and spaceship designs, to bio-engineering, with the simulation of blood flow on vessels and organs boosting the development of new medical procedures and bio-mechanical devices. However, computation of fluid flow problems can be a challenging task since it depends, e.g., on a robust technique to describe and approximate the governing equations, and a suitable representation of the computational domain, which can easily lead to a problem in the order of millions degrees of freedom.

In CFD analysis, applying reduced order models can also be difficult, since these problems can present strong nonlinearities and multiscale phenomena, which may not be properly reproduced by a low rank basis. Nevertheless, model order reduction has been the subject of many researchers for solving several

*Corresponding author

Email addresses: jwdfernandes@gmail.com (Jeferson Wilian Dossa Fernandes), rodolfo.sanches@usp.br (Rodolfo André Kuche Sanches), andrea.barbarulo@centralesupelec.fr (Andrea Barbarulo)

physical problems, including CFD, in the last decades. The main idea of this family of methods is to represent a complex problem involving a great number of variables by means of a reduced basis. Reduced order modeling can also be sorted in two classes: *a posteriori* and *a priori* methods. In the former, a reduced basis is built taking into account previous simulations of the full order model. Then, the reduced basis is projected to the governing equations, leading to an explicit reduced-order model. On the other hand, in the latter family of methods, separation of variables is employed to the problem unknowns, and these approximations are projected directly to the governing equations with no *a priori* knowledge on the solution.

Regarding CFD analysis, *a posteriori* methods, such as the Proper Orthogonal Decomposition (POD) and Reduced Basis (RB), were developed for solving Stokes flows in parameterized domains [1, 2], Navier-Stokes problems [3, 4] as well as fluid-structure modeling and flow control [5–9]. More recently, this family of methods was also explored in the simulation of complex flows involving moving boundaries [10, 11], for the simulation of turbulent flows by means of a residual-based variational multiscale (VMS) approach [12], considering porous media, rheology and non-Newtonian fluids [13], among other applications that can be found in the extensive literature review carried by Lassila et al. [14], Rowley and Dawson [15] and Mendonça et al. [16].

A priori techniques, such as the Proper Generalized Decomposition (PGD), have also been investigated in CFD analysis. For instance, the first approach for incompressible flows was presented by Dumon et al. [17], where a stream function-vorticity formulation was employed for the unsteady Navier-Stokes equations. Later, PGD approaches in a fractional step algorithm were also introduced, coupled to finite volume [18, 19] and spectral [20] discretizations, and also for parameterized incompressible flows in the OpenFOAM environment [21].

Space-time separated representations within PGD was firstly investigated by Ladevèze [22], with a non-incremental integration procedure. In the context of CFD, this concept was firstly employed by Aghighi et al. [23] for the simulation of transient nonlinear Navier-Stokes problems with temperature dependent density. On the other hand, an incremental PGD approach was also introduced by Dumon et al. [24] for the simulation of non-isothermal Navier-Stokes equations with mass transport in cavity flows.

In the work of Tamellini et al. [25], an alternative strategy suppressing the pressure terms employing spectral elements was presented for the stochastic steady incompressible Navier-Stokes equations. More recently, Le-Quoc et al. [26] developed an immersed boundary-PGD-based technique for incompressible flow modeling. The Navier-Stokes equations were solved in a fractional-step algorithm where PGD is applied for solving the Poisson’s equation needed for the pressure field updating.

Regarding the use of stabilized formulations, González et al. [27] have introduced the well known Streamline Upwind/Petrov-Galerkin (SUPG) strategy to the analysis of high-dimensional advection-diffusion equation within PGD. The authors have explored two versions of the stabilization technique, which have shown similar results. In the first one, the stabilization terms are introduced into the decomposed problem, while in the second PGD is applied directly to the stabilized weak form.

Although the collection of methods described before show important advances for the construction of PGD reduced order models for the simulation of incompressible flows, mixed formulations were few investigated in this context. It may be related to the strong enforcement of the incompressibility, the drawbacks of the LBB condition [28] and the difficulties on obtaining a PGD-reduced basis in this scenario. In this sense, the first PGD-mixed approach was presented by Díez et al. [29] for the parametric modeling of Stokes flows. The authors analyzed several options of the PGD solution separated forms with the application of a PGD compression algorithm based on a Least Squares projection to improve convergence. Later, Ghnatios and Hachem [30] presented a Galerkin Least Squares (GLS) stabilized mixed formulation for the simulation of Stokes flows. Finally, it is important to mention the significant advances achieved by Sevilla et al. [31] with the introduction of the isogeometric concept to PGD approximation of the Stokes equations within a mixed formulation.

In this work we extend the application of residual-based stabilized formulations to the transient Navier-Stokes equations, more specifically, the Pressure-Stabilizing/Petrov-Galerkin (PSPG) [32] approach, **which can be viewed as a PSPG version of formulation 1 in [27] applied to incompressible flows.** Stabilized mixed formulations are a class of consistent Finite Element techniques that have proven to be robust as they circumvent the LBB condition [28] allowing the use of equal-order interpolations for both velocity and pressure, while provide a better conditioned system, enhancing performance on the use of iterative solvers. Although widely employed on CFD analysis, in spite of the advances achieved in the last years on model order reduction, this family of methods are still few explored in this context. The reduced order model proposed introduces a space-time PGD for two-dimensional flows providing an alternative for the simulation of **moderate (maybe change moderate to low?)** Reynolds number laminar flows.

The paper is organized as follows: Section 2 presents the incompressible flow governing equations as well as the spatial discretization employing the PSPG residual-based formulation. In Section 3 the space-time decomposition is introduced and the PGD reduced basis is built. A set of numerical tests is presented in 4 in order to evaluate the proposed methodology. Conclusions and further discussions are drawn in Section 5.

2. Governing equations

Incompressible flows are modeled by the Navier-Stokes equations and may be stated as: find the velocity $\mathbf{u}(\mathbf{x}, t)$ and pressure $p(\mathbf{x}, t)$ fields, where \mathbf{x} refers to an arbitrary point of the computational domain $\Omega_{\mathbf{x}}$, i.e., $\mathbf{x} \in \Omega_{\mathbf{x}}$ and $t \in \Omega_t = [0, T]$ is an instant in the time domain Ω_t , such that

$$\rho \left(\frac{\partial \mathbf{u}}{\partial t} + \mathbf{u} \cdot \nabla \mathbf{u} - \mathbf{f} \right) - \nabla \cdot \boldsymbol{\sigma} = \mathbf{0} \quad (1)$$

and

$$\nabla \cdot \mathbf{u} = 0, \quad (2)$$

where ρ , \mathbf{f} , \mathbf{u} and $\boldsymbol{\sigma}$ are, respectively, the fluid density, body force, velocity field and the Cauchy stress tensor, given by

$$\boldsymbol{\sigma}(\mathbf{u}, p) = -p\mathbf{I} + 2\mu\boldsymbol{\varepsilon}(\mathbf{u}), \quad (3)$$

with p denoting the pressure field, \mathbf{I} the identity tensor, μ the fluid dynamic viscosity and the strain rate $\boldsymbol{\varepsilon}(\mathbf{u}) = (\nabla\mathbf{u} + \nabla\mathbf{u}^T)/2$.

The problem statement is completed by taking into account initial as well as Dirichlet and Neumann boundary conditions on portions Γ_D and Γ_N , respectively, of the computational domain boundary $\Gamma = \Gamma_D \cup \Gamma_N$, defined as

$$\mathbf{u}(\mathbf{x}, t = 0) = \mathbf{u}^0(\mathbf{x}) \text{ in } \Omega_x, \quad (4)$$

$$\mathbf{u} = \mathbf{g} \text{ on } \Gamma_D \quad (5)$$

and

$$\boldsymbol{\sigma}\mathbf{n} = \mathbf{h} \text{ on } \Gamma_N, \quad (6)$$

where \mathbf{n} represents the outward unit vector, \mathbf{g} and \mathbf{h} are known functions and \mathbf{u}_0 the initial velocity field, assumed to be divergence free, i.e., $\nabla \cdot \mathbf{u}_0 = 0$.

As it is well known, mixed formulations must satisfy the LBB or *inf-sup* condition [28] in order to yield a well-posed problem. However, in the past decades numerous techniques have been developed for circumventing the LBB condition [32–34]. One of the most successful, the residual-based Pressure-Stabilizing/Petrov-Galerkin (PSPG)[32] consists in modifying the test functions in a suitable and consistent way, enhancing stability. For further considerations over stabilized formulations, see for instance [32, 33, 35–39]. In the sense of residual-based stabilized formulations, the governing equations weak form is directly derived in the finite dimensional form, where the superscript h denotes a standard finite element discretization, such as

$$\int_{\Omega_x} \mathbf{w}^h \cdot \rho \left(\frac{\partial \mathbf{u}^h}{\partial t} + \mathbf{u}^h \cdot \nabla \mathbf{u}^h - \mathbf{f}^h \right) d\mathbf{x} + \int_{\Omega_x} \boldsymbol{\varepsilon}(\mathbf{w}^h) : \boldsymbol{\sigma}(\mathbf{u}^h, p^h) d\mathbf{x} - \int_{\Gamma_N} \mathbf{w}^h \cdot \mathbf{h}^h d\mathbf{x} = 0 \quad (7)$$

and

$$\int_{\Omega_x} q^h \nabla \cdot \mathbf{u}^h d\mathbf{x} + \sum_{e=1}^{n_{el}} \int_{\Omega^e} \tau_{\text{PSPG}} \left(\frac{\nabla q^h}{\rho} \right) \cdot \mathbf{r}_M(\mathbf{u}^h, p^h) d\mathbf{x} = 0, \quad (8)$$

where \mathbf{w}^h and q^h are test functions, τ_{PSPG} is a stabilization parameter, n_{el} is the number of finite elements in the domain discretization and $\mathbf{r}_M(\mathbf{u}^h, p^h)$ is the residual of the momentum equation. Therefore we adopt

$$\mathbf{r}_M(\mathbf{u}^h, p^h) = \rho \left(\frac{\partial \mathbf{u}^h}{\partial t} + \mathbf{u}^h \cdot \nabla \mathbf{u}^h - \mathbf{f}^h \right) - \nabla \cdot \boldsymbol{\sigma}(p^h, \mathbf{u}^h). \quad (9)$$

The proper definition of τ_{PSPG} has been the topic of an extensive investigation by many researchers in the past decades. The more recent works (see e.g. [38, 40] and references therein) have adopted nonlinear expressions to derive τ_{PSPG} , dependent on the velocity field, in the same sense as other well known residual-based stabilizations such as the Streamline-Upwind/Petrov-Galerkin (SUPG) and the Least Square Incompressibility Constraint (LSIC). Nonetheless, a simpler alternative solution consists on taking an element-level constant value of τ_{PSPG} , dependent on the finite element discretization such as in [32, 33]. This choice is particularly indicated in our case since the nonlinear terms in the governing equations are reduced and is given by

$$\tau_{\text{PSPG}} = \frac{\alpha^e h^e}{2\mu}, \quad (10)$$

where α^e is an arbitrary real positive constant and h^e is the characteristic element size, taken as the diameter of a circle with the same element area.

It can also be noticed from (8) that this strategy includes velocity second-order derivatives to the weak formulation. These terms vanish for linear finite element basis functions, and are often neglected for higher-order finite elements [35].

Under such considerations the time-continuous FEM approach of (7)-(8) can be written in a matrix form as

$$\begin{bmatrix} \mathbb{M} & \mathbf{0} \\ \mathbb{B} & \mathbf{0} \end{bmatrix} \begin{Bmatrix} \dot{\mathbf{U}} \\ \dot{\mathbf{p}} \end{Bmatrix} + \begin{bmatrix} \mathbb{K} + \mathbb{C}(\mathbf{u}^h) & \mathbb{G} \\ \mathbb{G}^T + \mathbb{V}(\mathbf{u}^h) & \mathbb{Q} \end{bmatrix} \begin{Bmatrix} \mathbf{U} \\ \mathbf{p} \end{Bmatrix} = \begin{Bmatrix} \mathbf{F} \\ \mathbf{D} \end{Bmatrix}, \quad (11)$$

with the FEM sub-matrices explicitly described in Appendix A. Notice that, in the case of a velocity-dependent definition of τ_{PSPG} , the terms \mathbb{B} , \mathbb{Q} and \mathbf{D} are also nonlinear, while \mathbb{V} is derived from the convective portion of the residual and is always dependent on \mathbf{u}^h .

3. PGD Algorithm

The PGD reduced basis is built over a separated space-time decomposition of velocity and pressure fields given by

$$\mathbf{u}^h(\mathbf{x}, t) \approx \sum_{j=1}^{N_{mod}} \mathcal{U}_j(\mathbf{x}) \circ \Phi_j(t) \quad (12)$$

and

$$p^h(\mathbf{x}, t) \approx \sum_{j=1}^{N_{mod}} \mathcal{P}_j(\mathbf{x}) \cdot \Psi_j(t), \quad (13)$$

where \circ refers to the element-wise (Hadamard) product and N_{mod} is the number of PGD modes, unknown *a priori*.

Both space and time functions are approximated in a FEM context, such that $\mathcal{U}_j(\mathbf{x}) = N^u(\mathbf{x})\mathbf{U}_j$, $\mathcal{P}_j(\mathbf{x}) = N^p(\mathbf{x})\mathcal{P}_j$, $\Phi_j(t) = N^t(t)\Phi_j$ and $\Psi_j(t) = N^t(t)\Psi_j$, where N^u , N^p and N^t are, respectively, the velocity, pressure and time finite element basis functions and \mathbf{U}_j , \mathcal{P}_j , Φ_j and Ψ_j refers to the nodal values of \mathcal{U}_j , \mathcal{P}_j , Φ_j and Ψ_j , respectively.

3.1. PGD enrichment step

The PGD couple is constructed iteratively by means of a fixed-point algorithm. The first stage of this process is described in this section. To ease the comprehension on the notation used in subsequent developments, we define the indexes n and k which refers to the current PGD mode and fixed-point iteration, respectively.

Thus, at a certain point of the computation, for a given PGD mode n , the velocity and pressure solution fields can be written as

$$\mathbf{u}_n^h(\mathbf{x}, t) = \sum_{i=1}^{n-1} \mathcal{U}_i(\mathbf{x}) \circ \Phi_i(t) + \mathcal{U}_n^{(k)}(\mathbf{x}) \circ \Phi_n^{(k)}(t) = \mathbf{u}_{n-1}^h(\mathbf{x}, t) + \mathcal{U}_n^{(k)}(\mathbf{x}) \circ \Phi_n^{(k)}(t), \quad (14)$$

and

$$p_n^h(\mathbf{x}, t) = \sum_{i=1}^{n-1} \mathcal{P}_i(\mathbf{x}) \cdot \Psi_i(t) + \mathcal{P}_n^{(k)}(\mathbf{x}) \cdot \Psi_n^{(k)}(t) = p_{n-1}^h(\mathbf{x}, t) + \mathcal{P}_n^{(k)}(\mathbf{x}) \cdot \Psi_n^{(k)}(t). \quad (15)$$

It is important to mention that both, initial velocity and pressure fields, respectively $\mathbf{u}^0(\mathbf{x}, 0)$, and $p^0(\mathbf{x}, 0)$, as well as Dirichlet boundary conditions, namely \mathbf{g} , may be introduced in the space-time decomposition (14)-(15). This will include analogous additional terms in the formulation, but are omitted in the following developments for the sake of simplicity and in order to avoid cumbersome expressions, without loss of generality.

Then, the PGD couple is obtained by employing the alternating direction strategy (see e.g. [41]), which states that for a given fixed point iteration k , obtaining the n -th pair of PGD modes $\mathcal{U}_n \circ \Phi_n$ and $\mathcal{P}_n \cdot \Psi_n$ is performed in two steps:

1) Compute the spatial modes $\mathcal{U}_n^{(k)}$ e $\mathcal{P}_n^{(k)}$ from previously computed time modes $\Phi_n^{(k-1)}$ and $\Psi_n^{(k-1)}$:

At this point, the solution for velocity and pressure fields (14)-(15), respectively, can be represented by

$$\mathbf{u}_n^h(\mathbf{x}, t) = \mathbf{u}_{n-1}^h(\mathbf{x}, t) + \mathcal{U}_n^{(k)}(\mathbf{x}) \circ \Phi_n^{(k-1)}(t), \quad (16)$$

and

$$p_n^h(\mathbf{x}, t) = p_{n-1}^h(\mathbf{x}, t) + \mathcal{P}_n^{(k)}(\mathbf{x}) \cdot \Psi_n^{(k-1)}(t). \quad (17)$$

Following the alternating direction algorithm, the natural choice [42] for the weighting functions \mathbf{w}^h and q^h are

$$\mathbf{w}^h = \delta \mathbf{u}^h = \delta \mathcal{U}_n(\mathbf{x}) \circ \Phi_n^{(k-1)}(t) \quad (18)$$

and

$$q^h = \delta p^h = \delta \mathcal{P}_n(\mathbf{x}) \cdot \Psi_n^{(k-1)}(t). \quad (19)$$

Introducing (16)-(17) and (18)-(19) onto the governing equations (7)-(8), assuming that the convective velocity \mathbf{u}^h is also known and making use of the FEM matrices previously described, one obtain the so-called *space problem*, given by

$$\begin{bmatrix} \mathbb{S}_{11} & \mathbb{S}_{12} \\ \mathbb{S}_{21} & \mathbb{S}_{22} \end{bmatrix} \begin{Bmatrix} \mathcal{U}_n^{(k)} \\ \mathcal{P}_n^{(k)} \end{Bmatrix} = \begin{Bmatrix} \mathbf{R}_1 - \mathbf{Z}_1 \\ \mathbf{R}_2 - \mathbf{Z}_2 \end{Bmatrix} \quad (20)$$

where

$$\mathbb{S}_{11} = \int_{\Omega_t} \Phi_n^{(k-1)} \mathbb{M} \dot{\Phi}_n^{(k-1)} dt + \int_{\Omega_t} \Phi_n^{(k-1)} [\mathbb{K} + \mathbb{C}(\mathbf{u}^h)] \Phi_n^{(k-1)} dt, \quad (21)$$

$$\mathbb{S}_{12} = \int_{\Omega_t} \Phi_n^{(k-1)} \mathbb{G} \Psi_n^{(k-1)} dt, \quad (22)$$

$$\mathbb{S}_{21} = \int_{\Omega_t} \Psi_n^{(k-1)} \mathbb{B} \dot{\Phi}_n^{(k-1)} dt + \int_{\Omega_t} \Psi_n^{(k-1)} [\mathbb{G}^T + \mathbb{V}(\mathbf{u}^h)] \Phi_n^{(k-1)} dt, \quad (23)$$

$$\mathbb{S}_{22} = \int_{\Omega_t} \Psi_n^{(k-1)} \mathbb{Q} \Psi_n^{(k-1)} dt, \quad (24)$$

$$\mathbf{R}_1 = \int_{\Omega_t} \Phi_n^{(k-1)} \mathbf{F}(t) dt, \quad (25)$$

$$\mathbf{R}_2 = \int_{\Omega_t} \Psi_n^{(k-1)} \mathbf{D}(t) dt, \quad (26)$$

$$\mathbf{Z}_1 = \sum_{i=1}^{n-1} \left[\int_{\Omega_t} \Phi_n^{(k-1)} \mathbb{M} \dot{\Phi}_i dt - \int_{\Omega_t} \Phi_n^{(k-1)} [\mathbb{K} + \mathbb{C}(\mathbf{u}^h)] \Phi_i dt \right] \mathcal{U}_i - \sum_{i=1}^{n-1} \left[\int_{\Omega_t} \Phi_n^{(k-1)} \mathbb{G} \Psi_i dt \right] \mathcal{P}_i \quad (27)$$

and

$$\mathbf{Z}_2 = \sum_{i=1}^{n-1} \left[\int_{\Omega_t} \Psi_n^{(k-1)} \mathbb{B} \dot{\Phi}_i dt + \int_{\Omega_t} \Psi_n^{(k-1)} [\mathbb{G}^T + \mathbb{V}(\mathbf{u}^h)] \Phi_i dt \right] \mathcal{U}_i + \sum_{i=1}^{n-1} \left[\int_{\Omega_t} \Psi_n^{(k-1)} \mathbb{Q} \Psi_i dt \right] \mathcal{P}_i. \quad (28)$$

From problem (20), spatial modes $\mathcal{U}_n^{(k)}$ and $\mathcal{P}_n^{(k)}$ are updated and the PGD enrichment step advances to the time modes computation.

2) Compute the temporal modes $\Phi_n^{(k)}$ and $\Psi_n^{(k)}$ from the updated spatial modes $\mathcal{U}_n^{(k)}$ and $\mathcal{P}_n^{(k)}$:

Analogously to the previous step, at this stage velocity and pressure fields can be expressed by

$$\mathbf{u}_n^h(\mathbf{x}, t) = \mathbf{u}_{n-1}^h(\mathbf{x}, t) + \mathcal{U}_n^{(k)}(\mathbf{x}) \circ \Phi_n^{(k)}(t) \quad (29)$$

and

$$p_n^h(\mathbf{x}, t) = p_{n-1}^h(\mathbf{x}, t) + \mathcal{P}_n^{(k)}(\mathbf{x}) \cdot \Psi_n^{(k)}(t). \quad (30)$$

On the other hand, following the alternating directions algorithm, \mathbf{w}^h and q^h are taken as

$$\mathbf{w}^h = \delta \mathbf{u}^h = \mathcal{U}_n^{(k)}(\mathbf{x}) \circ \delta \Phi_n(t) \quad (31)$$

and

$$q^h = \delta p^h = \mathcal{P}_n^{(k)}(\mathbf{x}) \cdot \delta \Psi_n(t). \quad (32)$$

Thus, introducing (29)-(30) and (31)-(32) into (7)-(8) and making use of the same FEM machinery, one obtain the so-called *time problem* given by

$$\begin{bmatrix} \dot{t}_{11} & 0 \\ \dot{t}_{21} & 0 \end{bmatrix} \begin{Bmatrix} \dot{\Phi}_n^{(k)} \\ \dot{\Psi}_n^{(k)} \end{Bmatrix} + \begin{bmatrix} t_{11} & t_{12} \\ t_{21} & t_{22} \end{bmatrix} \begin{Bmatrix} \Phi_n^{(k)} \\ \Psi_n^{(k)} \end{Bmatrix} = \begin{Bmatrix} r_1 - z_1 \\ r_2 - z_2 \end{Bmatrix} \quad (33)$$

where

$$\dot{t}_{11} = \mathbf{U}_n^{(k)T} \mathbb{M} \mathbf{U}_n^{(k)}, \quad (34)$$

$$\dot{t}_{21} = \mathcal{P}_n^{(k)T} \mathbb{B} \mathbf{U}_n^{(k)}, \quad (35)$$

$$t_{11} = \mathbf{U}_n^{(k)T} [\mathbb{C}(\mathbf{u}^h) + \mathbb{K}] \mathbf{U}_n^{(k)}, \quad (36)$$

$$t_{12} = \mathbf{U}_n^{(k)T} \mathbb{G} \mathcal{P}_n^{(k)}, \quad (37)$$

$$t_{21} = \mathcal{P}_n^{(k)T} [\mathbb{V}(\mathbf{u}^h) + \mathbb{G}^T] \mathbf{U}_n^{(k)}, \quad (38)$$

$$t_{22} = \mathcal{P}_n^{(k)T} \mathbb{Q} \mathcal{P}_n^{(k)}, \quad (39)$$

$$r_1 = \mathbf{u}_n^{(k)T} \mathbf{F}(t), \quad (40)$$

$$r_2 = \mathcal{P}_n^{(k)T} \mathbf{D}(t), \quad (41)$$

$$z_1 = \sum_{i=1}^{n-1} \left[\mathbf{u}_n^{(k)T} \mathbb{M} \mathbf{u}_i \dot{\Phi}_i(t) + \mathbf{u}_n^{(k)T} [\mathbb{K} + \mathbb{C}(\mathbf{u}^h)] \mathbf{u}_i \Phi_i(t) - \mathbf{u}_n^{(k)T} \mathbb{G} \mathcal{P}_i \Psi_i(t) \right] \quad (42)$$

and

$$z_2 = \sum_{i=1}^{n-1} \left[\mathcal{P}_n^{(k)T} \mathbb{B} \mathbf{u}_i \dot{\Phi}_i(t) + \mathcal{P}_n^{(k)T} [\mathbb{G}^T + \mathbb{V}(\mathbf{u}^h)] \mathbf{u}_i \Phi_i(t) + \mathcal{P}_n^{(k)T} \mathbb{Q} \mathcal{P}_i \Psi_i(t) \right]. \quad (43)$$

The time problem (33) is a system of ordinary differential equation and, in the developments presented in this work, implicit Euler scheme is employed to solve it incrementally as it is well known to be unconditionally stable (see for instance [43, 44]).

3.2. Linearization

At this stage let us focus on the treatment of the nonlinear terms $\mathbb{C}(\mathbf{u}^h)$ and $\mathbb{V}(\mathbf{u}^h)$. Two different choices have been generally used for the linearization of the convective term [23, 45]. The first and simplest one consists of linearizing the nonlinear terms explicitly from the previous PGD enrichment steps, namely

$$\mathbf{u}_n^h \cdot \nabla \mathbf{u}_n^h \approx \mathbf{u}_{n-1}^h \cdot \nabla \mathbf{u}_n^h. \quad (44)$$

As discussed in details by [23, 45], this choice is not optimal since the number of terms in the decomposition may be affected by the convergence rate of the fixed point iteration process on the PGD enrichment step as well as approximation errors. Another alternative, less sensitive to the fixed point algorithm convergence rate [23, 45], consists of an incremental linearization process, which takes into account the enrichment functions just computed in the previous fixed point iteration, i.e.,

$$\mathbf{u}_n^h \cdot \nabla \mathbf{u}_n^h \approx \left(\mathbf{u}_{n-1}^h + \mathcal{U}_n^{(k-1)} \circ \Phi_n^{(k-1)} \right) \cdot \nabla \left(\mathbf{u}_{n-1}^h + \mathcal{U}_n^{(k-1)} \circ \Phi_n^{(k-1)} \right). \quad (45)$$

The two options differ in the sense that, in the former, \mathbf{u}^h is not updated throughout the fixed-point algorithm while in the latter \mathbf{u}^h , $\mathbb{C}(\mathbf{u}^h)$ and $\mathbb{V}(\mathbf{u}^h)$ need to be updated at each iteration k . The second option provides a better approximation for the nonlinear terms by taking into account the current PGD mode, but implies in the re-computation of all nonlinear portion throughout the PGD enrichment step, increasing substantially the computational cost. For this reason, we follow the procedure adopted by Favoretto et al. [46], which consists in computing the first PGD couple by incremental (45) and the remaining PGD modes by explicit (44) linearizations.

3.3. PGD update step

Once the convergence criterion in the fixed-point algorithm is reached, a new couple $\mathcal{U}_n \circ \Phi_n$ and $\mathcal{P}_n \cdot \Psi_n$ is established. At this point, to ensure the orthogonality of the PGD basis, the new pair of space functions is subjected to a Gram-Schmidt orthonormalization procedure, taking into account the previous PGD modes. With this change, all time functions also need to be updated. This procedure follows the same idea of Favoretto et al. [46].

With the orthogonalization process, the partial PGD solution is given by $\mathbf{u}^h = \bar{\mathcal{U}}_i \circ \Phi_i$ and $p^h = \bar{\mathcal{P}}_i \cdot \Psi_i$, for $i = 1, \dots, n$, where $\bar{\mathcal{U}}_i$ and $\bar{\mathcal{P}}_i$ refers to an orthogonal vector basis.

Finally, projecting the partial solution into the governing equations results in

$$\sum_{i,j=1}^n \bar{\mathcal{U}}_j^T \mathbb{M} \bar{\mathcal{U}}_i \dot{\Phi}_i + \sum_{i,j=1}^n \bar{\mathcal{U}}_j^T [\mathbb{C}(\mathbf{u}^h) + \mathbb{K}] \bar{\mathcal{U}}_i \Phi_i + \sum_{i,j=1}^n \bar{\mathcal{U}}_j^T \mathbb{G} \bar{\mathcal{P}}_i \Psi_i = \sum_{j=1}^n \bar{\mathcal{U}}_j^T \mathbf{F}(t) \quad (46)$$

and

$$\sum_{i,j=1}^n \bar{\mathcal{P}}_j^T \mathbb{B} \bar{\mathcal{U}}_i \dot{\Phi}_i + \sum_{i,j=1}^n \bar{\mathcal{P}}_j^T [\mathbb{V}(\mathbf{u}^h) + \mathbb{G}^T] \bar{\mathcal{U}}_i \Phi_i + \sum_{i,j=1}^n \bar{\mathcal{P}}_j^T \mathbb{Q} \bar{\mathcal{P}}_i \Psi_i = \sum_{j=1}^n \bar{\mathcal{P}}_j^T \mathbf{D}(t). \quad (47)$$

Problem (46)-(47) is analogous to the *time problem* in the PGD enrichment step and allows to recompute all time functions incrementally by the implicit Euler method.

The developments previously presented are summarized in the Algorithm 1. In addition, the fixed-point iteration needs to be initialized by a given value of $\Phi_n^{(0)}$ and $\Psi_n^{(0)}$, which are taken as linear functions.

4. Numerical tests

In this section a set of numerical tests are presented in order to evaluate the proposed formulation. In all cases the space modes are approximated by P2P2 finite elements, i.e., triangles with quadratic approximation for both velocity and pressure fields. Time modes are also approximated by quadratic functions.

4.1. Stokes problem

In this first example we consider a simple problem modeled by the Stokes equations, obtained by suppressing the convective terms in (7)-(8), leading to the variational problem given by

$$\int_{\Omega_{\mathbf{x}}} \mathbf{w}^h \cdot \rho \left(\frac{\partial \mathbf{u}^h}{\partial t} - \mathbf{f}^h \right) d\mathbf{x} + \int_{\Omega_{\mathbf{x}}} \boldsymbol{\varepsilon}(\mathbf{w}^h) : \boldsymbol{\sigma}(\mathbf{u}^h, p^h) d\mathbf{x} - \int_{\Gamma_N} \mathbf{w}^h \cdot \mathbf{h}^h d\mathbf{x} = 0 \quad (48)$$

and

$$\int_{\Omega_{\mathbf{x}}} q^h \nabla \cdot \mathbf{u}^h d\mathbf{x} + \sum_{e=1}^{n_{e1}} \int_{\Omega_{\mathbf{x}}^e} \tau_{\text{PSPG}} \left(\frac{\nabla q^h}{\rho} \right) \cdot \mathbf{r}_M(\mathbf{u}^h, p^h) d\mathbf{x} = 0, \quad (49)$$

with $\mathbf{r}_M(\mathbf{u}^h, p^h)$ given by

Algorithm 1 Stabilized Navier-Stokes space-time PGD

Require: $\mathbb{M}, \mathbb{K}, \mathbb{G}, \mathbb{G}^T, \mathbf{F}(t), \mathbb{B}, \mathbb{Q}, \mathbf{D}(t)$, boundary and initial conditions;

```

1: for  $n = 1$  to  $N_{mod}$  do
2:    $k=0$ ;
3:   - Initialize  $\Phi_n^{(0)}$  and  $\Psi_n^{(0)}$ .
4:   if  $n \geq 2$  then
5:     - Nonlinear enrichment: Compute  $\mathbf{u}^h, \mathbb{C}(\mathbf{u}^h)$  and  $\mathbb{V}(\mathbf{u}^h)$ ;
6:   end if
7:   while  $\varepsilon_{PGD} \downarrow tol_{PGD}$  do
8:      $k++$ ;
9:     if  $n=1$  then
10:      - Nonlinear enrichment: Compute  $\mathbf{u}^h, \mathbb{C}(\mathbf{u}^h)$  and  $\mathbb{V}(\mathbf{u}^h)$ ;
11:    end if
12:    PGD enrichment step:
13:    - Space problem: Compute  $\mathcal{U}_n^{(k)}$  and  $\mathcal{P}_n^{(k)}$  from  $\Phi_n^{(k-1)}$  and  $\Psi_n^{(k-1)}$  known, i.e., solve (20);
14:    - Time problem: Compute  $\Phi_n^{(k)}$  and  $\Psi_n^{(k)}$  from  $\mathcal{U}_n^{(k)}$  and  $\mathcal{P}_n^{(k)}$  known, i.e., solve (33);
15:    - Compute  $\varepsilon_{PGD} = \min(\varepsilon_u, \varepsilon_p)$ , such that
      
$$\varepsilon_u = \frac{2 \int_T (\Phi_n^k - \Phi_n^{k-1})^2 dt}{\int_T (\Phi_n^k + \Phi_n^{k-1})^2 dt} \quad \text{and} \quad \varepsilon_p = \frac{2 \int_T (\Psi_n^k - \Psi_n^{k-1})^2 dt}{\int_T (\Psi_n^k + \Psi_n^{k-1})^2 dt};$$

16:  end while
17:  PGD update step:
18:  - Space modes  $\mathcal{U}_n$  and  $\mathcal{P}_n$  orthogonalization (Gram-Schmidt process);
19:  - Update step: Re-computation of all time functions  $\left\{ \begin{array}{l} \Phi_1, \dots, \Phi_n \\ \Psi_1, \dots, \Psi_n \end{array} \right\}$ ;
20: end for

```

$$\mathbf{r}_M(\mathbf{u}^h, p^h) = \rho \left(\frac{\partial \mathbf{u}^h}{\partial t} - \mathbf{f}^h \right) - \nabla \cdot \boldsymbol{\sigma}(p^h, \mathbf{u}^h). \quad (50)$$

If the following source term is taken

$$\mathbf{f} = \begin{cases} (1 - 2\pi)(8\pi^2\nu - 1) \cos(2\pi x) \sin(2\pi y) e^{-t} \\ (1 + 2\pi)(1 - 8\pi^2\nu) \cos(2\pi y) \sin(2\pi x) e^{-t} \end{cases}, \quad (51)$$

the problem has analytic solution given by

$$\mathbf{u}_a = \begin{cases} \cos(2\pi x) \sin(2\pi y) e^{-t} \\ -\sin(2\pi x) \cos(2\pi y) e^{-t} \end{cases} \quad (52)$$

and

$$p_a = (1 - 8\pi^2\nu) \cos(2\pi x) \sin(2\pi y) e^{-t}, \quad (53)$$

where $\nu = \mu/\rho$ is the kinematic viscosity.

The analysis is performed over a square domain $\Omega_{\mathbf{x}} = [0.25; 0.50] \times [1.25; 1.50]$ with boundary and initial conditions directly derived by (52)-(53). ρ and ν are taken, respectively, as 1.0 and 0.01 and the stabilization parameter τ_{PSPG} is computed with $\alpha^e = 0.05$, empirically chosen (see [33] for more details). All variables are also taken in the non-dimensional form.

The first test consists of a convergence analysis over the spatial discretization. In this case the time step is fixed in $\Delta t = 0.001$ and the time interval $\Omega_t = [0, 1]$. All variables are considered dimensionless. The simulations are performed increasing progressively n_h , the number of nodes in each direction of the structured finite element discretization.

In the context of PGD analysis, this problem was also investigated by Dumon et al. [18], which have employed the following norms to evaluate the convergence

$$e_u = \|\mathbf{u}^h - \mathbf{u}_a\|_{L^\infty(L^2(\Omega_{\mathbf{x}}))} = \max_{0 < t \leq T} \left[\int_{\Omega_{\mathbf{x}}} |\mathbf{u}^h - \mathbf{u}_a|^2 d\mathbf{x} \right]^{\frac{1}{2}} \quad (54)$$

and

$$e_p = \|p^h - p_a\|_{L^2(L^2(\Omega))} = \left[\int_T \int_{\Omega} |p^h - p_a|^2 d\Omega dT \right]^{\frac{1}{2}}. \quad (55)$$

The same error norms e_u and e_p are employed in this work.

As one can notice, the analytical solution (52)-(53) describes a time exponential decay of constant velocity and pressure profiles. In this case, we take 2 PGD modes for both pressure and velocity. The obtained results are presented in Fig. 1.

In the work of Dumon et al. [18] the PGD reduced basis is built over a fractional-step approach, which splits the full coupled equations in two sub-problems, one to obtain velocity and other to obtain pressure

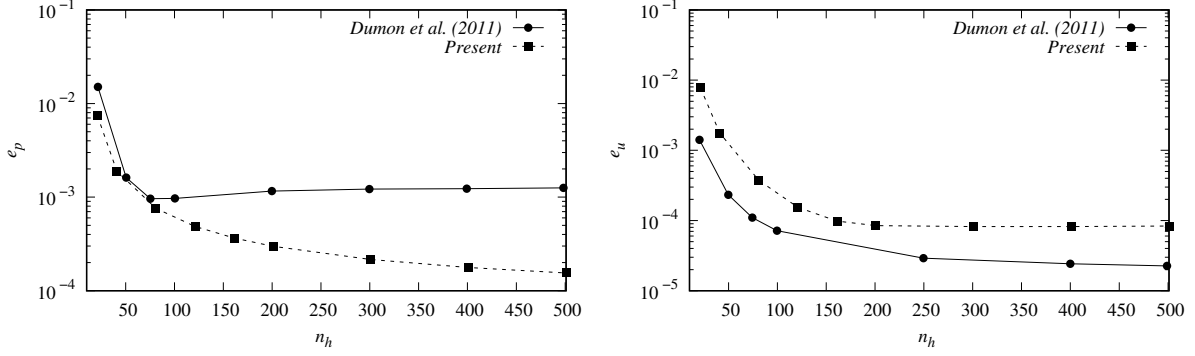


Figure 1: Stokes problem: velocity and pressure spatial convergence.

fields. In the present work, with mixed approach, both variables are kept coupled in a single problem, which may explain the better convergence obtained for the pressure field. On the other hand, slightly higher values of e_u were obtained for the velocity fields. This can be due to the definition of e_u that takes the maximum time-discrete value of the $L^2(\Omega_{\mathbf{x}})$ norm.

Following, we perform a second convergence analysis regarding time discretization. In this case four different time steps are chosen: $\Delta t = 0.001, 0.005, 0.01$ and 0.02 , whose results are presented in Fig. 2.

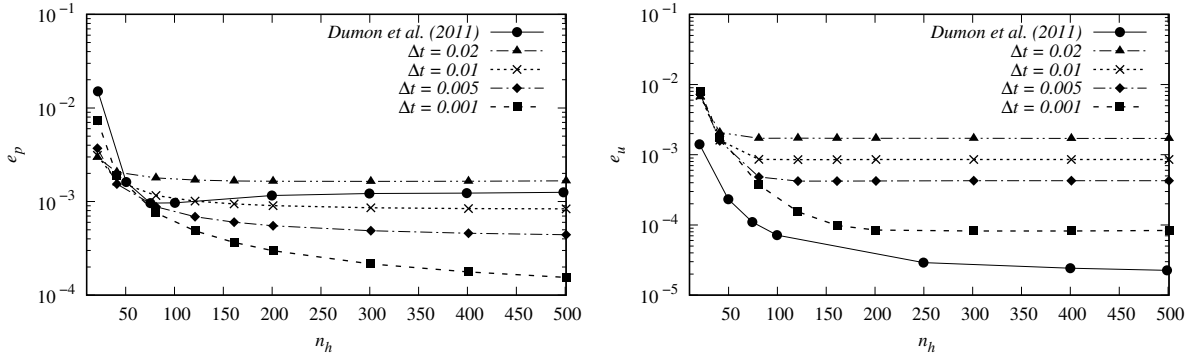
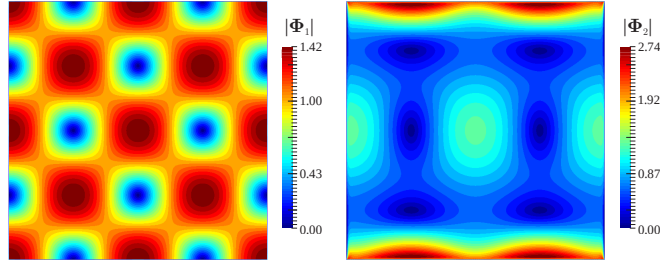


Figure 2: Stokes problem: velocity and pressure convergence for different Δt .

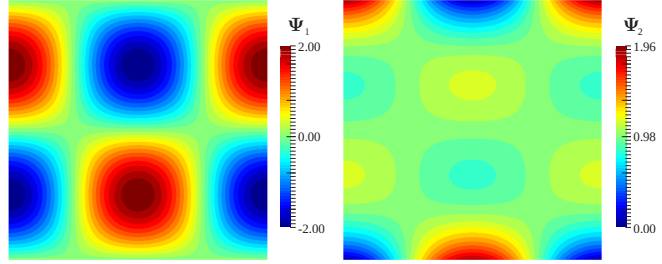
For the case of $\Delta t = 0.001$ and $n_h = 501$, the PGD space (Fig. 3) and time (Fig. 4) modes are presented. The PGD solution at $t = 1$ is also presented in Fig. 5. In the case of time modes, it can be noticed that both Φ_2 and Ψ_2 present much lower magnitude than Φ_1 and Ψ_1 , respectively, showing that a single pair of PGD modes is sufficient to represent the flow behavior in this case. It can also be observed in Fig. 6 which plots the convergence of velocity and pressure fields related to the number of PGD couples.

4.2. Taylor-Green problem

In the following numerical tests the flow complexity is gradually increased and nonlinear cases are explored. Similarly to the previous one, the Taylor-Green problem is a benchmark of unsteady flow with decaying vortex, which presents the general analytical solution for the Navier-Stokes equations given by



(a) Velocity space modes.



(b) Pressure space modes.

Figure 3: Stokes problem: space modes.

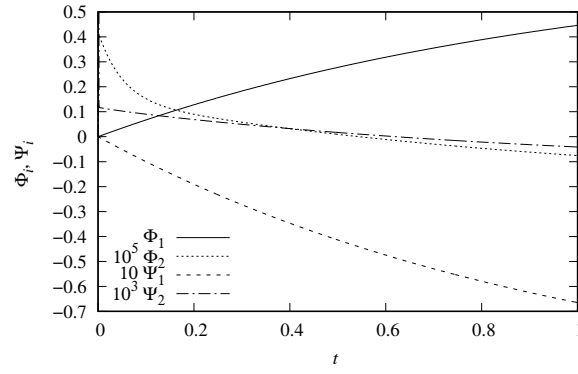


Figure 4: Stokes problem: time modes.

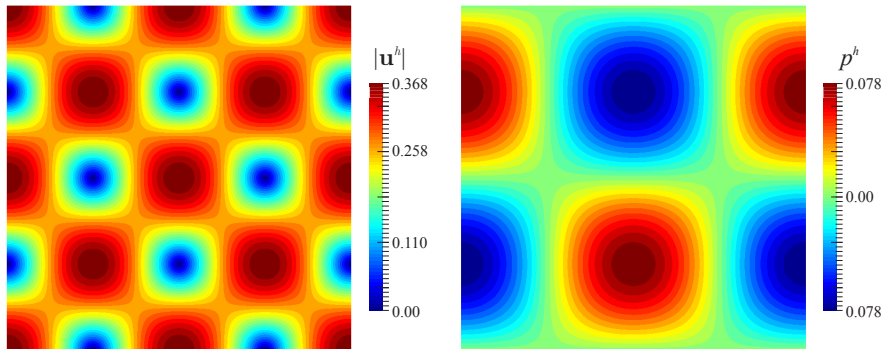


Figure 5: Stokes problem: velocity and pressure fields at $t = 1$.

$$\mathbf{u} = \begin{cases} -\cos(2\pi x) \sin(2\pi y) e^{-8\pi^2 \nu t} \\ \sin(2\pi x) \cos(2\pi y) e^{-8\pi^2 \nu t} \end{cases} \quad (56)$$

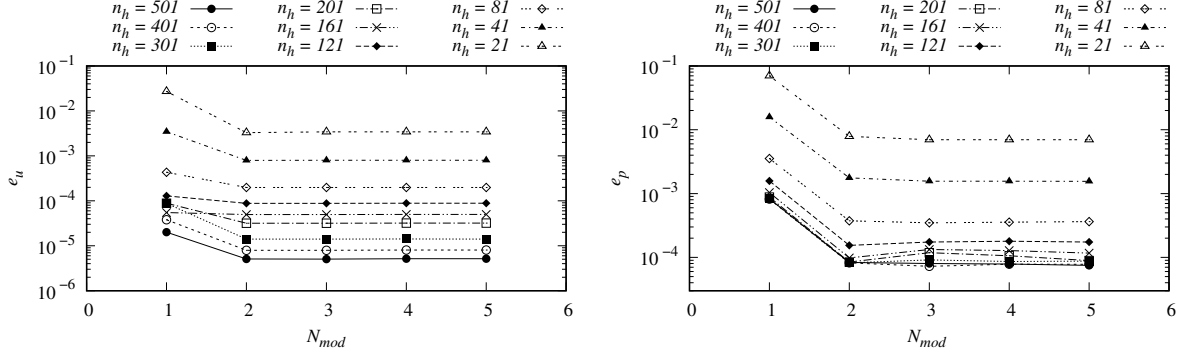


Figure 6: Stokes problem: velocity and pressure convergence as a function of N_{mod} .

and

$$p = -\frac{1}{4} (\cos(4\pi x) + \cos(4\pi y)) e^{-16\pi^2 \nu t}, \quad (57)$$

with $\mathbf{f} = \mathbf{0}$.

The solution is again performed in the square domain $\Omega_{\mathbf{x}} = [0.25; 0.50] \times [1.25; 1.50]$, with initial and boundary conditions derived by (56)-(57), $\rho=1.0$, $\nu = 0.01$ and $\Delta t = 0.001$. As in the previous example, the analytical solution describes constant velocity and pressure fields subjected to an exponential decay, allowing the adoption of two PGD modes to represent the solution.

In the first test we aim to evaluate the influence of the τ_{PSPG} stabilization parameter in the convergence over the spatial discretization. Thus, two definitions of τ_{PSPG} are taken in account: the constant element-level value of τ_{PSPG} given in (10) (with $\alpha^e=0.05$) and a nonlinear definition from [36] and [40], given by

$$\tau_{\text{PSPG}} = \left(\frac{1}{\tau_{\text{SUGN1}}^2} + \frac{1}{\tau_{\text{SUGN2}}^2} + \frac{1}{\tau_{\text{SUGN3}}^2} \right)^{-\frac{1}{2}}, \quad (58)$$

with

$$\tau_{\text{SUGN1}} = \left(\sum_{i=1}^{n_{\text{en}}} |\mathbf{u}^h \cdot \nabla N_i^u| \right)^{-1}, \quad (59)$$

$$\tau_{\text{SUGN2}} = \frac{\Delta t}{2}, \quad (60)$$

$$\tau_{\text{SUGN3}} = \frac{h_{\text{RGN}}^2}{4\nu}, \quad (61)$$

$$h_{\text{RGN}} = 2 \left(\sum_{i=1}^{n_{\text{en}}} |\mathbf{r} \cdot \nabla N_i^u| \right)^{-1} \quad (62)$$

and

$$\mathbf{r} = \frac{\nabla |\mathbf{u}^h|}{\|\nabla |\mathbf{u}^h|\|}, \quad (63)$$

where n_{en} is the number of element nodes.

This problem was also studied by Dumon [47] in the PGD fractional-step approach and the results obtained for both parameters as well as the reference values are presented in Fig. (7).

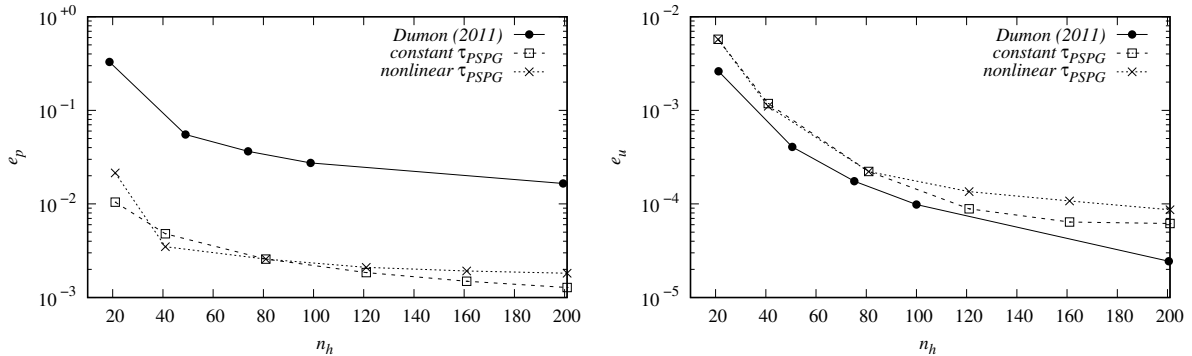


Figure 7: Taylor-Green problem: error analysis for constant and nonlinear definitions of τ_{PSPG} .

It is important to highlight that the adoption of a velocity-dependent definition of τ_{PSPG} increases the computational effort to obtain a reduced basis as more terms become nonlinear, for instance \mathbb{B} , \mathbb{Q} and \mathbb{D} . However, it may be noticed that, for both constant and nonlinear τ_{PSPG} , similar error values are obtained, which supports the choice of a more simple expression for its definition. In addition, the same pattern obtained for the Stokes problem is recovered in this case, with smaller pressure errors, similar velocity errors and close convergence rates in both cases compared to the reference .

In Figs. 8, 9 and 10 both, space and time, PGD modes are presented, as well as the solution at $t=1$.

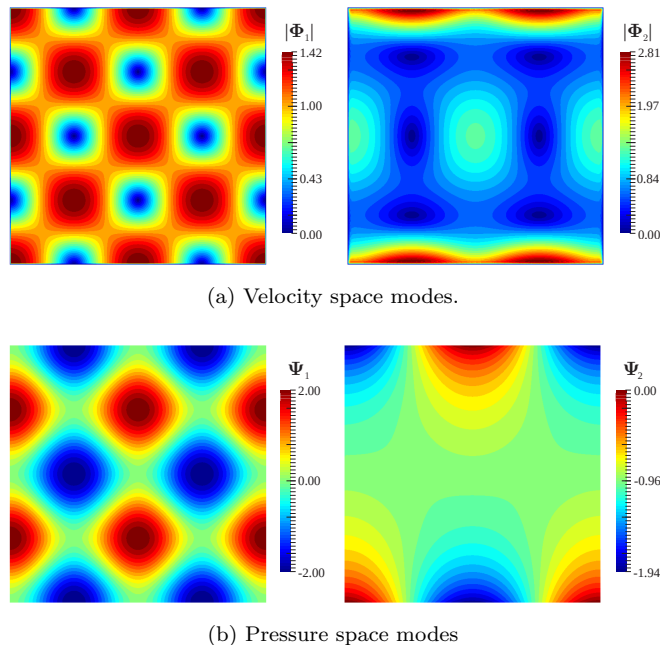


Figure 8: Taylor-Green problem: space modes.

Finally, the CPU time is also evaluated in this example. For this purpose, we have considered solutions

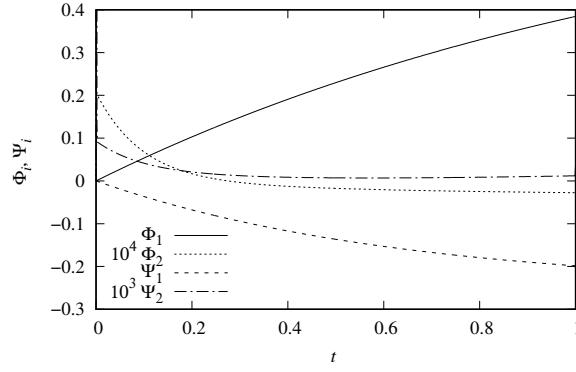


Figure 9: Taylor-Green problem: time modes.

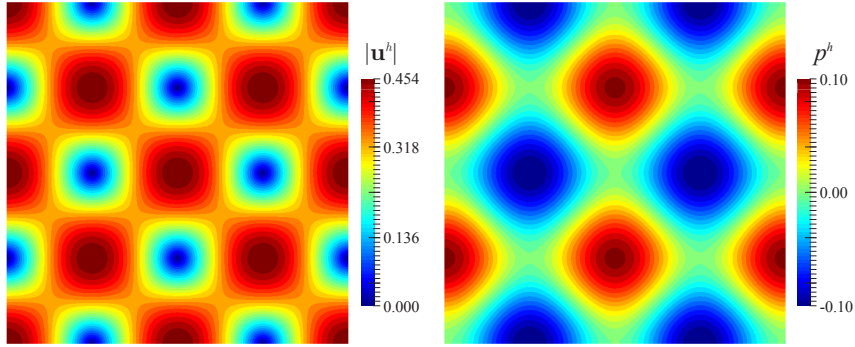


Figure 10: Taylor-Green problem: velocity and pressure fields at $t = 1$.

from 1 to 5 PGD modes and a standard FEM approach with the same spatial discretization. In addition, the nonlinear term in the FEM approach is approximated by means of the Newton's method. Both FEM and PGD implementations are performed in a MPI `parallel` environment and all simulations are carried in an Intel Xeon CPU E5-2640 v3 with 8 MPI processes. The results are presented in Fig. 11. As a matter of comparison, Fig 12 also presents the convergence as a function of the number of PGD couples for $n_h=201, 161$ and 121 .

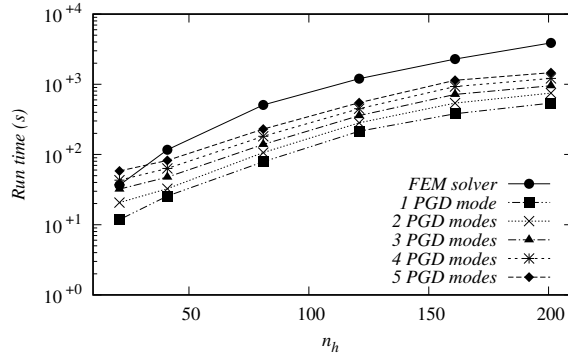


Figure 11: Taylor-Green problem: CPU time.

In standard FEM approaches the most time consuming task, in general, consists of assembling and solving the algebraic system of equations, solved 3-4 times per time step in average, which is the case

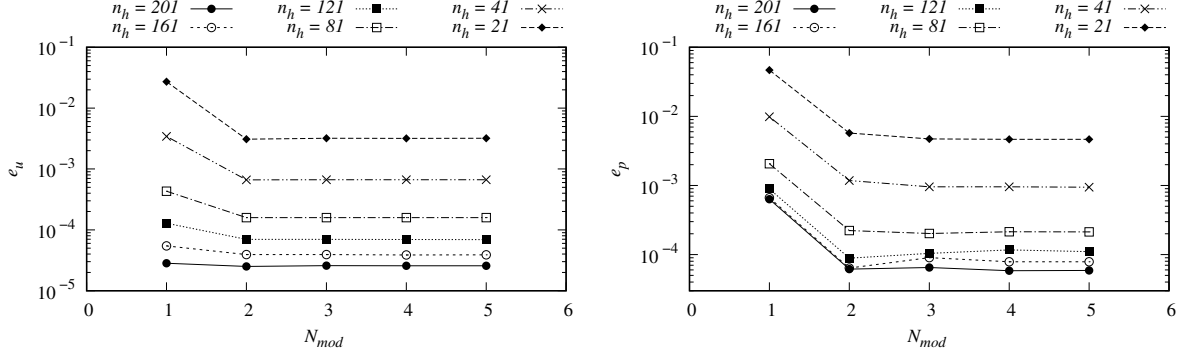


Figure 12: Taylor-Green problem: velocity and pressure convergence as a function of N_{mod} .

of the standard FEM model adopted, where the Jacobian operator is reconstructed at each Newton's iteration. In our PGD approach, most of the FE-based matrices are constant throughout the analysis and can be computed in a pre-process step. In addition, most of the operations can easily be carried at the element-level, and the full order linear system only needs to be solved at the *space problem* stage, which makes the PGD approach more scalable in terms of parallelization compared to standard FEM solvers.

Although the solution of this problem could be achieved with fewer number of PGD modes, even the solution with 5 PGD modes has shown to be 2.65 times faster than the full FEM model while the solution considered in the previous analysis is 5.18 times faster in the most refined model with $n_h=201$.

4.3. Lid-driven cavity

This example consists on the well known benchmark problem of a lid-driven cavity. It is a square domain fulfilled by fluid with a lid driven, which promotes the vortex formation inside the cavity. Both geometry and boundary conditions are illustrated in Fig. 13.

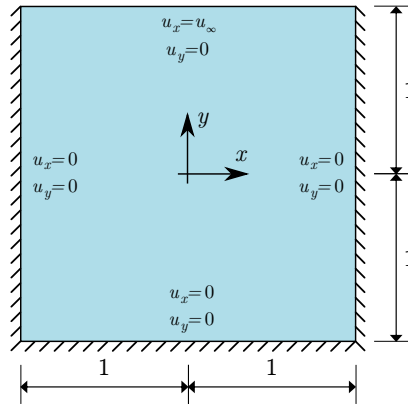


Figure 13: Lid-driven cavity: geometry and boundary conditions.

This problem is analyzed in four different scenarios: Reynolds numbers ($Re = u_\infty L/\nu$) equal to 100, 400, 1000 and 5000. Such values are computed taking the cavity side as characteristic length (L), unitary density and lid velocity ($\rho = u_\infty = 1$) and variable viscosity to achieve the respective Reynolds number.

In addition, all simulations are performed with 5 PGD modes. The computational domain is discretized with a structured finite element mesh with $n_h=201$, the time step is taken as $\Delta t = 0.05$ and the PSPG stabilization parameter is computed with $\alpha^e=0.05$.

As in usual finite element computations, the solution obtained for lower Reynolds numbers is used as initial field for the higher ones, in order to reduce the number of time steps needed to achieve the steady state solution, while for the case of $Re = 100$ the flow starts from rest.

Our results are evaluated by means of the velocity profiles u_y over the line $y = 0$ and u_x over the line $x=0$ and compared to the Ghia et al. [48] in Fig. 14. Velocity and pressure fields for the steady-state solution are also presented in Fig. 15 and 16, respectively, for $Re = 100, 400$ and 1000. In all cases the PGD results have shown to be in agreement with the reference values of [48].

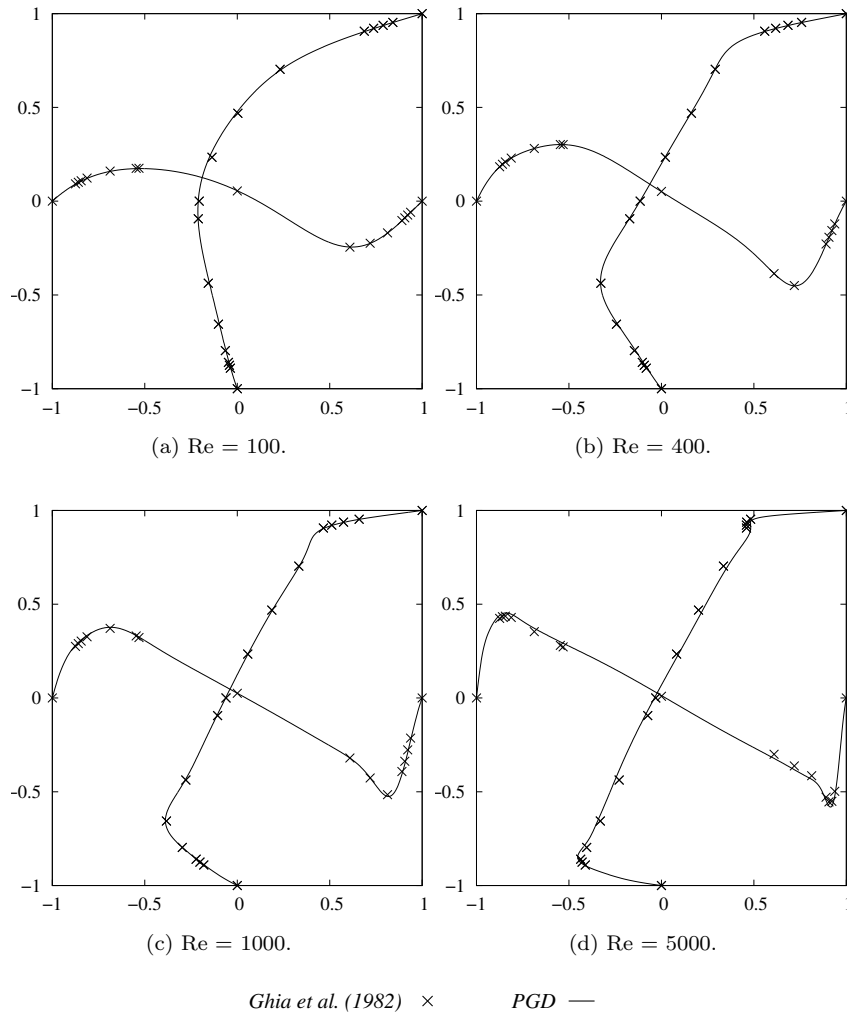


Figure 14: Lid-driven cavity: velocity profiles for u_x at $x = 0$ and for u_y at $y = 0$.

For the case of $Re = 5000$ we present in Figs. 17 and 18 the PGD velocity and pressure modes, that compose the solution. Notice that all time modes have an asymptotic behavior. If the magnitude of each temporal mode is taken at $t = T$, one can notice that the steady-state solution is mainly given by the first PGD mode. Approximately 85.41% and 89.83% of the steady-state velocity and pressure fields,

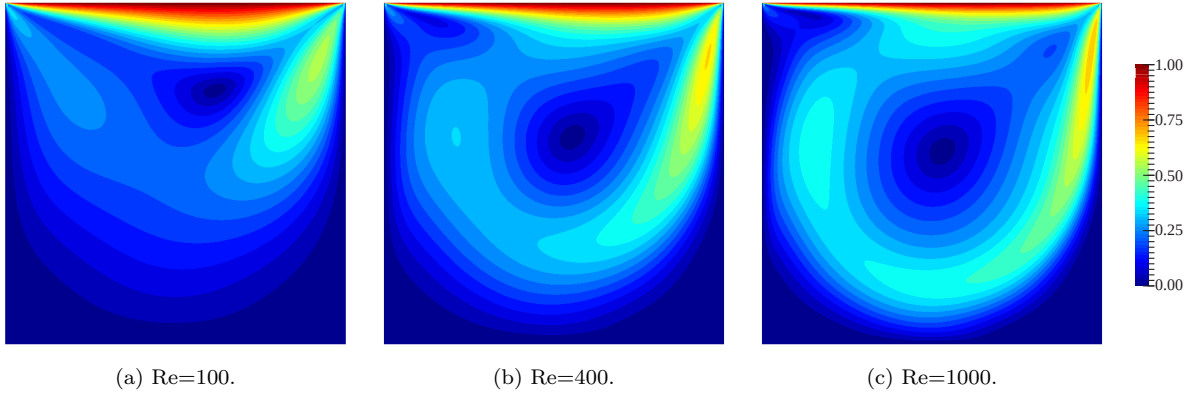


Figure 15: Lid-driven cavity: PGD velocity magnitude $|\mathbf{u}^h|$.

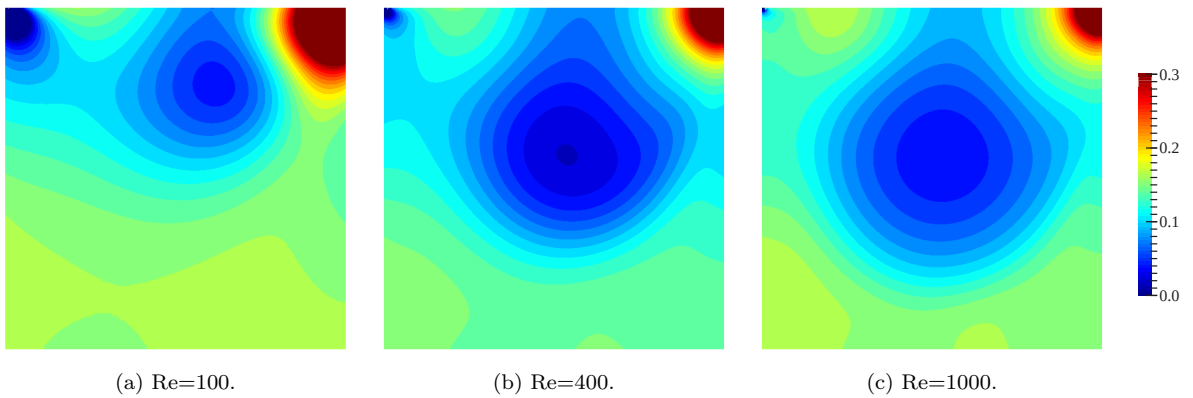


Figure 16: Lid-driven cavity: PGD pressure magnitude $|p^h|$.

respectively, are given by the first PGD mode. This major contribution of the first PGD mode can be attributed, e.g., to the nonlinear enrichment step, which in this case is performed at each fixed point iteration.

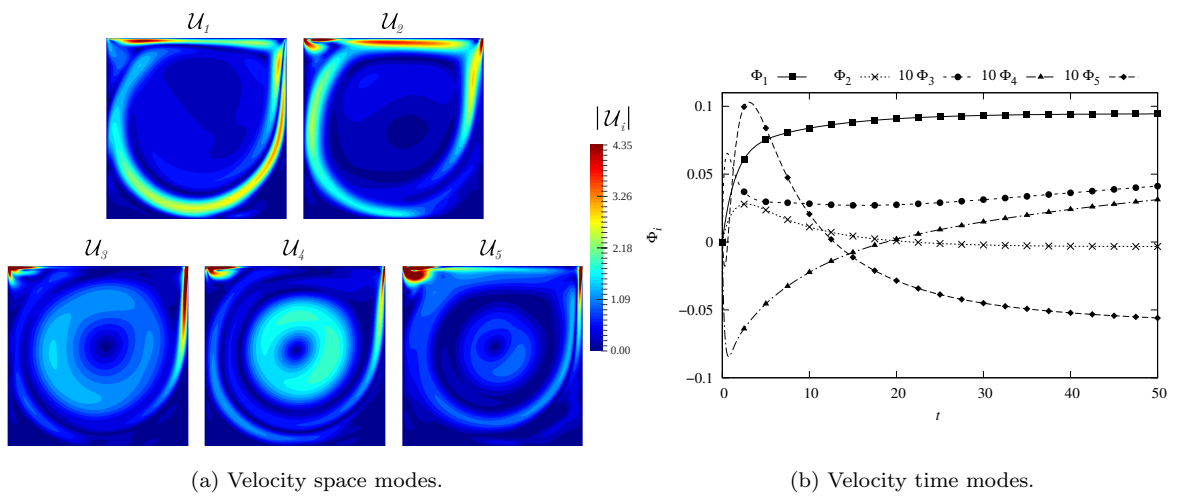


Figure 17: Lid-driven cavity: velocity space and time PGD modes for $\text{Re} = 5000$.

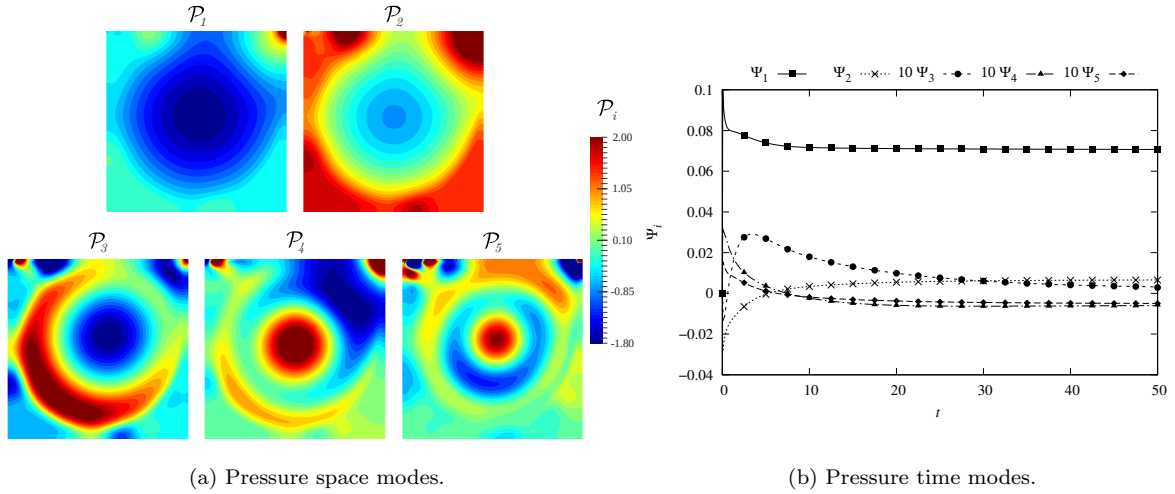


Figure 18: Lid-driven cavity: pressure space and time PGD modes for $Re = 5000$.

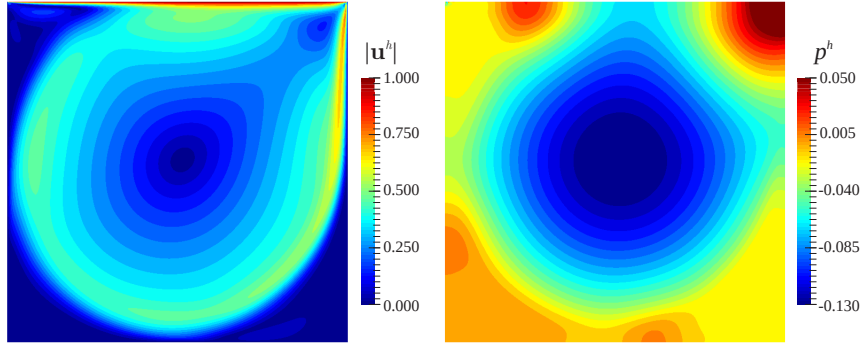


Figure 19: Lid-driven cavity: steady-state solution for $Re = 5000$.

4.4. Flow past a cylinder

In this example one evaluate the proposed formulation for the problem of a flow past a circular cylinder at low Reynolds numbers. In summary, two scenarios are evaluated: with $Re=30$ and 40 . In both cases the analysis start with the solution of a flow with $Re=1$. In addition, the simulation is performed with 200 time steps of $\Delta t = 0.1$ and taking $\alpha^e = 0.1$ and $N_{mod}=10$.

The computational domain consists on a rectangle $\Omega_x = [0, 0] \times [75, 20]$ with a unit-diameter circular cylinder vertically centered and 15 units far from the left edge. Uniform flow ($u_x = 1, u_y=0$) is prescribed at $x = 0$, symmetry (slip) boundary conditions are enforced at the upper and lower edges and free-stream velocity is prescribed at the upstream boundary.

The simulations are performed with an unstructured finite element mesh with 58,753 elements and 118,167 nodes. Results are evaluated by means of the pressure coefficient (C_p) at $t = 20$ as a function of θ , the angle from the uniform flow direction, as shown in Fig. 20. Moreover, the results are compared to the experimental data of Grove et al. [49] and the numerical simulations of Hamielec and Raal [50] and Sen et al. [51] and presented in Fig. 20. The comparison shows good agreement with the references, evidencing the PGD approach precision, specially when compared to the results of Sen et al. [51], which

have also employed a similar residual-based finite element formulation in their analysis.

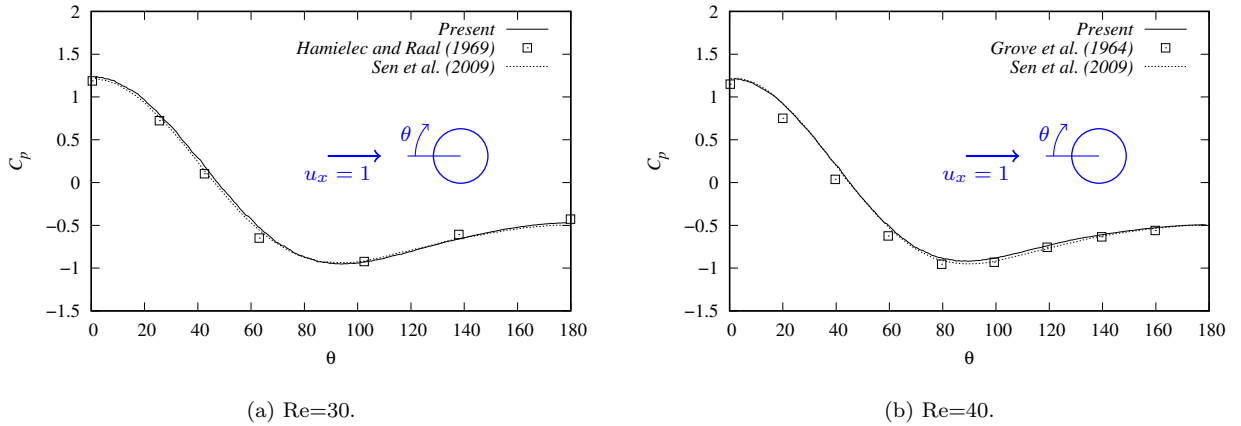


Figure 20: Flow past a cylinder: Pressure coefficient as a function of θ .

Similarly to the previous examples, for the case of $Re=30$, some spatial PGD couples as well as the time modes are presented in Figs. 21-22 and the steady-state solution at $t=1$ for both cases in Fig. 23.

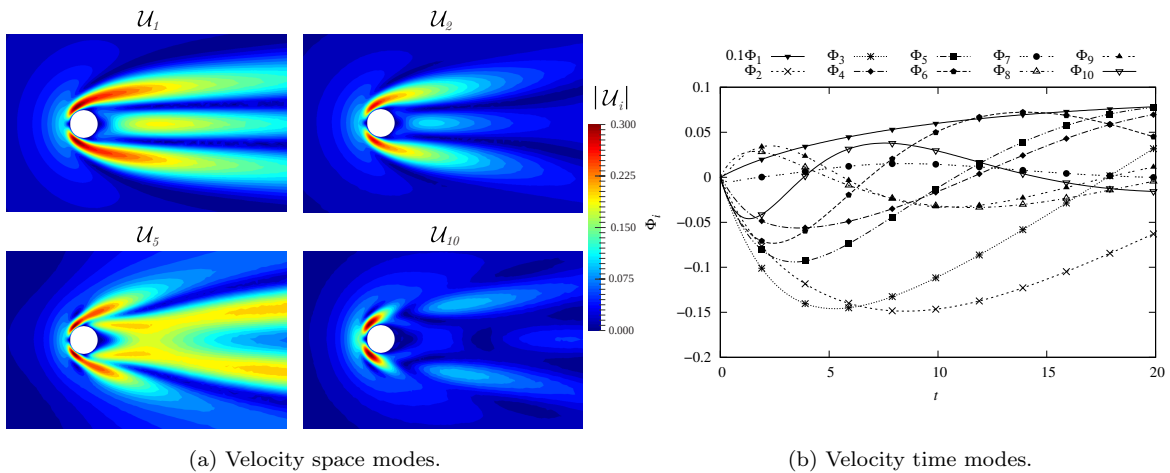


Figure 21: Flow past a cylinder: velocity space and time PGD modes for $Re = 30$.

5. Conclusions

In this work we have presented a PGD reduced order model for solving the transient incompressible Navier-Stokes equations with a residual-based stabilized finite element formulation. The proposed strategy was applied for solving cavity flow problems, showing that the PGD results are in agreement with the reference results for a range of Reynolds numbers from 100 to 5000, even with a reduced basis built over a low number of PGD couples, confirming its robustness and precision. This formulation also presents considerable CPU time saving compared to a full order finite element solver, as one can see from the numerical tests.

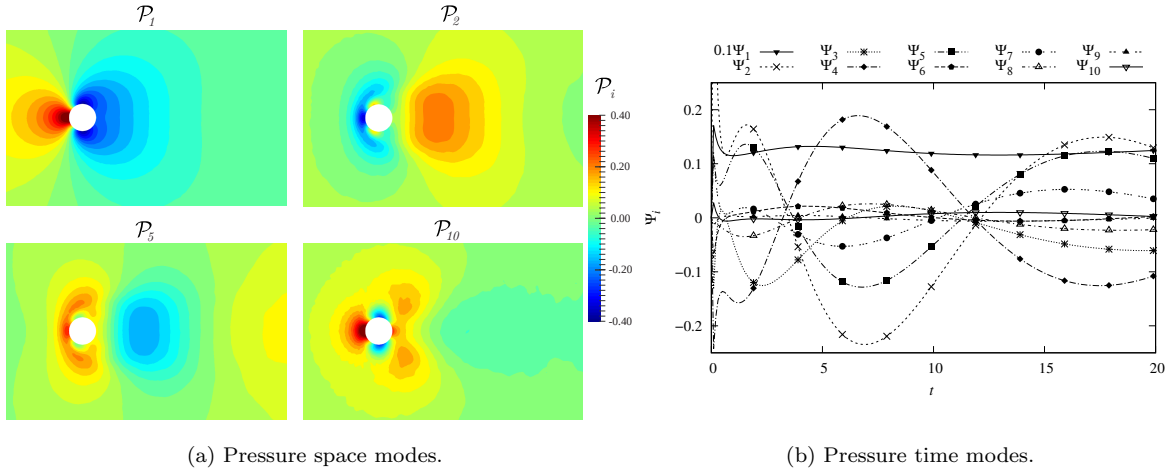


Figure 22: Flow past a cylinder: pressure space and time PGD modes for $Re = 30$.

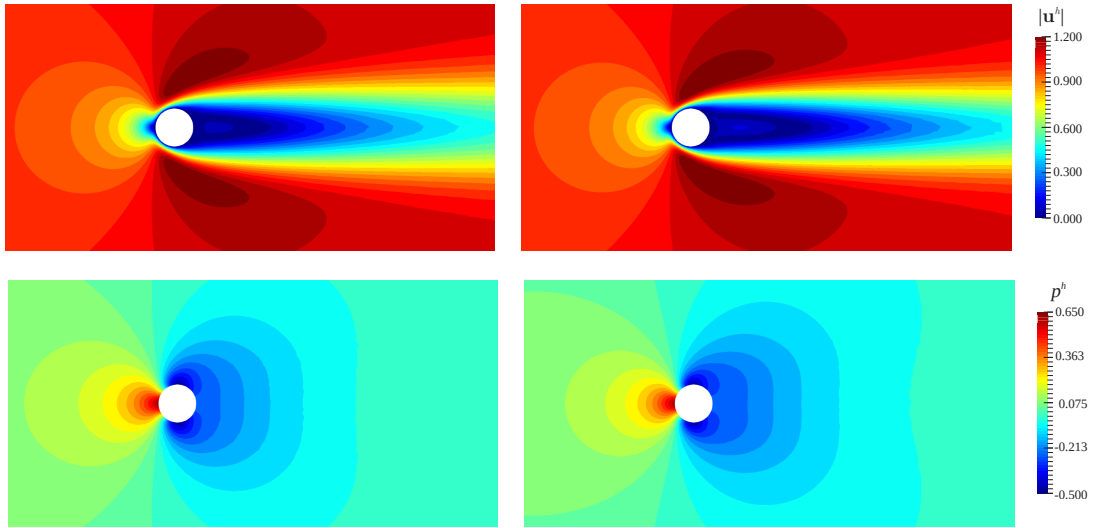


Figure 23: Flow past a cylinder: steady-state solution for $Re = 30$ (left) and $Re=40$ (right).

Finally, we consider this work as a first step on the use of PGD for the simulation of the transient Navier-Stokes equations in a fully implicit residual-based stabilized context, with focus in the application of the technique for 2D analysis, in order to evaluate its potential for both scientific and industrial large scale applications. In further developments this formulation should be extend to the 3D case, and improvements on the PGD algorithm for solving more complex problems, [such as convection-dominated flows](#).

Acknowledgments

This study was financed in part by the Coordenação de Aperfeiçoamento de Pessoal de Nível Superior – Brasil (CAPES) - Finance Code 001 and grant 88881.188582/2018-01. The authors are also grateful to the Brazilian National Council for Research and Technological Development (CNPq), grant 141015/2016-0.

Appendix A. Finite element sub-matrices

The sub-matrices derived from a Finite Element approximation of the PSPG-stabilized formulation of the Navier-Stokes equations are given by

$$\mathbb{M} = [\mathbf{M}_{ij}] = \int_{\Omega_{\mathbf{x}}} \rho N_i^u \cdot N_j^u \delta_{ab} \, d\mathbf{x}, \quad (\text{A.1})$$

$$\mathbb{K} = [\mathbf{K}_{ij}] = \int_{\Omega_{\mathbf{x}}} \mu \left[\nabla N_i^u \cdot \nabla N_j^u \delta_{ab} + \frac{\partial N_i^u}{\partial x_b} \frac{\partial N_j^u}{\partial x_a} \right] \, d\mathbf{x}, \quad (\text{A.2})$$

$$\mathbb{C}(\mathbf{u}^h) = [\mathbf{C}_{ij}] = \int_{\Omega_{\mathbf{x}}} \rho N_i^u \cdot \mathbf{u}^h \cdot \nabla N_j^u \delta_{ab} \, d\mathbf{x}, \quad (\text{A.3})$$

$$\mathbb{G} = [\mathbf{G}_{il}] = \int_{\Omega_{\mathbf{x}}} N_i^u \cdot \nabla N_l^p \, d\mathbf{x}, \quad (\text{A.4})$$

$$\mathbb{G}^T = [\mathbf{G}_{kj}] = \int_{\Omega_{\mathbf{x}}} N_k^p \nabla \cdot N_j^u \, d\mathbf{x}, \quad (\text{A.5})$$

$$\mathbf{F}(t) = [\mathbf{F}_j] = \int_{\Omega_{\mathbf{x}}} \rho N_j^u \cdot \mathbf{f}^h \, d\mathbf{x} + \int_{\Gamma_N} N_j^u \cdot \mathbf{h}^h \, d\mathbf{x}, \quad (\text{A.6})$$

$$\mathbb{B} = [\mathbf{B}_{kj}] = \sum_{e=1}^{n_{el}} \int_{\Omega_x^e} \tau_{\text{PSPG}} \nabla N_k^p \cdot N_j^u \, d\mathbf{x}, \quad (\text{A.7})$$

$$\mathbb{V}(\mathbf{u}^h) = [\mathbf{V}_{kj}] = \sum_{e=1}^{n_{el}} \int_{\Omega_x^e} \tau_{\text{PSPG}} \nabla N_k^p \cdot \mathbf{u}^h \cdot \nabla N_j^u \, d\mathbf{x}, \quad (\text{A.8})$$

$$\mathbb{Q} = [\mathbf{Q}_{kl}] = \sum_{e=1}^{n_{el}} \int_{\Omega_x^e} \frac{\tau_{\text{PSPG}}}{\rho} \nabla N_k^p \cdot \nabla N_l^p \, d\mathbf{x} \quad (\text{A.9})$$

and

$$\mathbf{D}(t) = [\mathbf{D}_l] = \sum_{e=1}^{n_{el}} \int_{\Omega_x^e} \tau_{\text{PSPG}} \nabla N_k^p \cdot \mathbf{f}^h \, d\mathbf{x}, \quad (\text{A.10})$$

where N^u and N^p are, respectively, velocity and pressure shape functions, i, j are velocity degrees of freedom, k, l are pressure degrees of freedom, δ_{ab} refers to the Kronecker delta and $a, b = 1, \dots, n_{sd}$ and with n_{sd} denoting the number of space dimensions.

References

- [1] G. Rozza, K. Veroy, On the stability of the reduced basis method for stokes equations in parametrized domains, *Computer Methods in Applied Mechanics and Engineering* 196 (2007) 1244 – 1260. URL: <https://doi.org/10.1016/j.cma.2006.09.005>.

- [2] G. Rozza, D. B. P. Huynh, A. Manzoni, Reduced basis approximation and a posteriori error estimation for stokes flows in parametrized geometries: roles of the inf-sup stability constants, *Numerische Mathematik* 125 (2013) 115–152. URL: <https://doi.org/10.1007/s00211-013-0534-8>.
- [3] A. Quarteroni, G. Rozza, Numerical solution of parametrized navier–stokes equations by reduced basis methods, *Numerical Methods for Partial Differential Equations* 23 (2007) 923–948. URL: <https://doi.org/10.1002/num.20249>.
- [4] A. Tallet, C. Allery, C. Leblond, E. Liberge, A minimum residual projection to build coupled velocity–pressure pod–rom for incompressible navier–stokes equations, *Communications in Nonlinear Science and Numerical Simulation* 22 (2015) 909 – 932. URL: <https://doi.org/10.1016/j.cnsns.2014.09.009>.
- [5] E. H. Dowell, K. C. Hall, Modeling of fluid-structure interaction, *Annu. Rev. Fluid Mech.* 33 (2001) 445–490. URL: <https://doi.org/10.1146/annurev.fluid.33.1.445>.
- [6] K. Kunisch, S. Volkwein, Galerkin proper orthogonal decomposition methods for parabolic problems, *Numer. Math.* 90 (2001) 117–148. URL: <https://doi.org/10.1007/s002110100282>.
- [7] M. Hinze, S. Volkwein, Proper orthogonal decomposition surrogate models for nonlinear dynamical systems: Error estimates and suboptimal control, in: P. Benner, V. Mehrmann, D. Sorensen (Eds.), *Lecture Notes in Computational and Applied Mathematics*, volume 45, Springer, Berlin, Heidelberg, 2005, pp. 261–306. URL: https://doi.org/10.1007/3-540-27909-1_10.
- [8] T. Lieu, C. Farhat, M. Lesoinne, Reduced-order fluid/structure modeling of a complete aircraft configuration, *Computer Methods in Applied Mechanics and Engineering* 195 (2006) 5730 – 5742. URL: <https://doi.org/10.1016/j.cma.2005.08.026>, john H. Argyris Memorial Issue. Part II.
- [9] K. Kunisch, S. Volkwein, Optimal snapshot location for computing POD basis functions, *ESAIM: Mathematical Modelling and Numerical Analysis* 44 (2010) 509–529. URL: <https://doi.org/10.1051/m2an/2010011>.
- [10] E. Liberge, A. Hamdouni, Reduced order modelling method via proper orthogonal decomposition (POD) for flow around an oscillating cylinder, *Journal of Fluids and Structures* 26 (2010) 292 – 311. URL: <https://doi.org/10.1016/j.jfluidstructs.2009.10.006>.
- [11] E. N. Karatzas, G. Stabile, L. Nouveau, G. Scovazzi, G. Rozza, A reduced basis approach for PDEs on parametrized geometries based on the shifted boundary finite element method and application to a Stokes flow, *Computer Methods in Applied Mechanics and Engineering* 347 (2019) 568 – 587. URL: <https://doi.org/10.1016/j.cma.2018.12.040>.
- [12] G. Stabile, F. Ballarin, G. Zuccarino, G. Rozza, A reduced order variational multiscale approach for turbulent flows, *Advances in Computational Mathematics* (2019). URL: <https://doi.org/10.1007/s10444-019-09712-x>.

- [13] F. Chinesta, A. Ammar, A. Leygue, R. Keunings, An overview of the proper generalized decomposition with applications in computational rheology, *Journal of Non-Newtonian Fluid Mechanics* 166 (2011) 578 – 592. URL: <https://doi.org/10.1016/j.jnnfm.2010.12.012>, xVIth International Workshop on Numerical Methods for Non-Newtonian Flows.
- [14] T. Lassila, A. Manzoni, A. Quarteroni, G. Rozza, *Model Order Reduction in Fluid Dynamics: Challenges and Perspectives*, Springer International Publishing, Cham, 2014, pp. 235–273. URL: https://doi.org/10.1007/978-3-319-02090-7_9.
- [15] C. W. Rowley, S. T. Dawson, *Model Reduction for Flow Analysis and Control*, *Annual Review of Fluid Mechanics* 49 (2017) 387–417. URL: [10.1146/annurev-fluid-010816-060042](https://doi.org/10.1146/annurev-fluid-010816-060042).
- [16] G. Mendonça, F. Afonso, F. Lau, *Model order reduction in aerodynamics: Review and applications*, *Proceedings of the Institution of Mechanical Engineers, Part G: Journal of Aerospace Engineering* 233 (2019) 5816–5836. URL: [10.1177/0954410019853472](https://doi.org/10.1177/0954410019853472).
- [17] A. Dumon, C. Allery, A. Ammar, *Proper Generalized Decomposition method for incompressible flows in stream-vorticity formulation*, *European Journal of Computational Mechanics* 19 (2010) 591–617. URL: [10.3166/ejcm.19.591-617](https://doi.org/10.3166/ejcm.19.591-617).
- [18] A. Dumon, C. Allery, A. Ammar, *Proper general decomposition (pgd) for the resolution of navier–stokes equations*, *Journal of Computational Physics* 230 (2011) 1387 – 1407. URL: <https://doi.org/10.1016/j.jcp.2010.11.010>.
- [19] C. Leblond, C. Allery, *A priori space–time separated representation for the reduced order modeling of low reynolds number flows*, *Computer Methods in Applied Mechanics and Engineering* 274 (2014) 264 – 288. URL: <https://doi.org/10.1016/j.cma.2014.02.010>.
- [20] A. Dumon, C. Allery, A. Ammar, *Proper generalized decomposition method for incompressible navier–stokes equations with a spectral discretization*, *Applied Mathematics and Computation* 219 (2013) 8145 – 8162. URL: <https://doi.org/10.1016/j.amc.2013.02.022>.
- [21] V. Tsiolakis, M. Giacomini, R. Sevilla, C. Othmer, A. Huerta, *Nonintrusive proper generalised decomposition for parametrised incompressible flow problems in OpenFOAM*, *Computer Physics Communications* 249 (2020) 107013. URL: <https://doi.org/10.1016/j.cpc.2019.107013>.
- [22] P. Ladevèze, *On algorithm family in structural mechanics. [sur une famille d’algorithmes en mecanique des structures.]*, *Comptes rendus des seances de l’Academie des sciences. Serie 2, Mecanique, Physique, Chimie, Sciences de la Terre, Sciences de l’univers* 300 (1985) 41–44.
- [23] M. Aghighi, A. Ammar, C. Metivier, M. Normandin, F. Chinesta, *Non-incremental transient solution of the Rayleigh–Bénard convection model by using the PGD*, *Journal of Non-Newtonian Fluid Mechanics* 200 (2013) 65–78. URL: <https://doi.org/10.1016/j.jnnfm.2012.11.007>.

- [24] A. Dumon, C. Allery, A. Ammar, Simulation of Heat and Mass Transport in a Square Lid-Driven Cavity with Proper Generalized Decomposition (PGD), *Numerical Heat Transfer, Part B: Fundamentals* 63 (2013) 18–43. URL: [10.1080/10407790.2012.724991](https://doi.org/10.1080/10407790.2012.724991).
- [25] L. Tamellini, O. Le Maître, A. Nouy, Model reduction based on proper generalized decomposition for the steady incompressible Navier-Stokes equations, *Siam Journal on Scientific Computing* 36 (2014) 29. A1089–A1117. URL: [10.1137/120878999](https://doi.org/10.1137/120878999).
- [26] C. Le-Quoc, L. A. Le, V. Ho-Huu, P. D. Huynh, T. Nguyen-Thoi, An immersed boundary proper generalized decomposition (ib-pgd) for fluid–structure interaction problems, *International Journal of Computational Methods* 15 (2018) 1850045. URL: [10.1142/S0219876218500457](https://doi.org/10.1142/S0219876218500457).
- [27] D. González, E. Cueto, F. Chinesta, P. Díez, A. Huerta, Streamline upwind/Petrov–Galerkin-based stabilization of proper generalized decompositions for high-dimensional advection–diffusion equations, *International Journal for Numerical Methods in Engineering* 94 (2013) 1216–1232. doi:<https://doi.org/10.1002/nme.4493>.
- [28] F. Brezzi, M. Fortin, *Mixed and hybrid finite element methods*, in: Vol. 15 of Springer Series in Computational Mathematics, Springer, New York, 1991.
- [29] P. Díez, S. Zlotnik, A. Huerta, Generalized parametric solutions in stokes flow, *Computer Methods in Applied Mechanics and Engineering* 326 (2017) 223 – 240. URL: <https://doi.org/10.1016/j.cma.2017.07.016>.
- [30] C. Ghnatios, E. Hachem, A stabilized mixed formulation using the proper generalized decomposition for fluid problems, *Computer Methods in Applied Mechanics and Engineering* 346 (2019) 769 – 787. URL: <https://doi.org/10.1016/j.cma.2018.09.030>.
- [31] R. Sevilla, S. Zlotnik, A. Huerta, Solution of geometrically parametrised problems within a CAD environment via model order reduction, *Computer Methods in Applied Mechanics and Engineering* 358 (2020) 112631. URL: <https://doi.org/10.1016/j.cma.2019.112631>.
- [32] T. E. Tezduyar, S. Mittal, S. E. Ray, R. Shih, Incompressible flow computations with stabilized bilinear and linear equal-order-interpolation velocity-pressure elements, *Comput. Methods Appl. Mech. Engrg.* 95 (1992) 221–242.
- [33] T. J. Hughes, L. P. Franca, M. Balestra, A new finite element formulation for computational fluid dynamics: V. Circumventing the Babuška-Brezzi condition: a stable Petrov-Galerkin formulation of the stokes problem accommodating equal-order interpolations, *Computer Methods in Applied Mechanics and Engineering* 59 (1986) 85 – 99. URL: [https://doi.org/10.1016/0045-7825\(86\)90025-3](https://doi.org/10.1016/0045-7825(86)90025-3).
- [34] T. J. Hughes, L. P. Franca, A new finite element formulation for computational fluid dynamics: Vii. the stokes problem with various well-posed boundary conditions: Symmetric formulations that

- converge for all velocity/pressure spaces, *Computer Methods in Applied Mechanics and Engineering* 65 (1987) 85 – 96. URL: [https://doi.org/10.1016/0045-7825\(87\)90184-8](https://doi.org/10.1016/0045-7825(87)90184-8).
- [35] T. E. Tezduyar, Y. Osawa, Finite element stabilization parameters computed from element matrices and vectors, *Computer Methods in Applied Mechanics and Engineering* 190 (2000) 411–430. URL: [https://doi.org/10.1016/S0045-7825\(00\)00211-5](https://doi.org/10.1016/S0045-7825(00)00211-5).
- [36] T. E. Tezduyar, Computation of moving boundaries and interfaces and stabilization parameters, *International Journal for Numerical Methods in Fluids* 43 (2003) 555–575. URL: <https://doi.org/10.1002/flid.505>.
- [37] T. Tezduyar, S. Sathe, Stabilization parameters in supg and pspg formulations, *Journal of Computational and Applied Mechanics* 4 (2003) 71–88.
- [38] K. Takizawa, T. E. Tezduyar, Y. Otaguro, Stabilization and discontinuity-capturing parameters for space–time flow computations with finite element and isogeometric discretizations, *Computational Mechanics* 62 (2018) 1169–1186. URL: <https://doi.org/10.1007/s00466-018-1557-x>.
- [39] J. W. D. Fernandes, A. Barbarulo, H. Ben Dhia, R. A. K. Sanches, A residual-based stabilized finite element formulation for incompressible flow problems in the Arlequin framework, *Computer Methods in Applied Mechanics and Engineering* 370 (2020) 113073.
- [40] Y. Bazilevs, K. Takizawa, T. E. Tezduyar, *Computational Fluid-Structure Interaction: Methods and Applications*, John Wiley & Sons, Chichester, UK, 2013.
- [41] F. Chinesta, R. Keunings, A. Leygue, *The Proper Generalized Decomposition for Advanced Numerical Simulations: A Primer*, Springer briefs in Applied Sciences and Technology, Springer, 2013. URL: <https://doi.org/10.1007/978-3-319-02865-1>, 132 p.
- [42] A. Nouy, A priori model reduction through Proper Generalized Decomposition for solving time-dependent partial differential equations, *Computer Methods in Applied Mechanics and Engineering* 199 (2010) 1603–1626.
- [43] J. Donea, A. Huerta, *Finite Element Methods for flow problems*, John Wiley & Sons, Chichester, UK, 2003.
- [44] T. J. R. Hughes, *The Finite Element Method: Linear Static and Dynamic Finite Element Analysis*, Prentice-Hall, Inc., Englewood Cliffs, NJ, 1987.
- [45] A. Ammar, M. Normandin, F. Daim, D. Gonzalez, E. Cueto, F. Chinesta, Non-incremental strategies based on separated representations: applications in computational rheology, *Commun. Math. Sci.* 8 (2010) 671–695.
- [46] B. Favoretto, C. A. Hillerin, O. Bettinotti, V. Oancea, A. Barbarulo, Reduced order modeling via pgd for highly transient thermal evolutions in additive manufacturing, *Computer Methods in Applied*

Mechanics and Engineering 349 (2019) 405 – 430. URL: <https://doi.org/10.1016/j.cma.2019.02.033>.

- [47] A. Dumon, Réduction dimensionnelle de type PGD pour la résolution des écoulements incompressibles, Thesis, Université de La Rochelle, La Rochelle, 2011.
- [48] U. Ghia, K. N. Ghia, C. T. Shin, High-Re solutions for incompressible flow using the Navier-Stokes equations and a multigrid method, *Journal of Computational Physics* 48 (1982) 387–441. URL: [https://doi.org/10.1016/0021-9991\(82\)90058-4](https://doi.org/10.1016/0021-9991(82)90058-4).
- [49] A. S. Grove, F. H. Shair, E. E. Petersen, An experimental investigation of the steady separated flow past a circular cylinder, *Journal of Fluid Mechanics* 19 (1964) 60–80. doi:[10.1017/S0022112064000544](https://doi.org/10.1017/S0022112064000544).
- [50] A. E. Hamielec, J. D. Raal, Numerical studies of viscous flow around circular cylinders, *The Physics of Fluids* 12 (1969) 11–17. URL: <https://aip.scitation.org/doi/abs/10.1063/1.1692253>. doi:[10.1063/1.1692253](https://doi.org/10.1063/1.1692253). arXiv:<https://aip.scitation.org/doi/pdf/10.1063/1.1692253>.
- [51] S. Sen, S. Mittal, G. Biswas, Steady separated flow past a circular cylinder at low reynolds numbers, *Journal of Fluid Mechanics* 620 (2009) 89–119. doi:[10.1017/S0022112008004904](https://doi.org/10.1017/S0022112008004904).